Int. J. Electrochem. Sci., 15 **(2020)** 6920 – 6929, doi: 10.20964/2020.07.67

International Journal of ELECTROCHEMICAL SCIENCE
www.electrochemsci.org

Study on the Preparation and Modification of $LiNi_{0.6}Co_{0.2}Mn_{0.2}O_2$ from spent Lithium ion Batteries as Lithium and Cobalt Source

Bowen He, Guanghui Guo[*]*, Ningsheng Zhang, Jie Wu, Jiaxin Zhu, Jianghua Qiu*

Key Laboratory of Hubei Province for Coal Conversion and New Carbon Materials, Wuhan University of Science and Technology, Wuhan 430081, China
[*]E-mall: guoguanghui@wust.edu.cn

Received: 31 December 2019 / *Accepted:* 4 May 2020 / *Published:* 10 June 2020

In this work, a process has been proposed to recover cobalt and lithium elements from spent $LiCoO_2$ batteries, then these elements were used as raw materials for the synthesis of $LiNi_{0.6}Co_{0.2}Mn_{0.2}O_2$ material. In addition, aluminum ion was selected as a dopant to modify the $LiNi_{0.6}Co_{0.2}Mn_{0.2}O_2$. The obtained materials were characterized by X-ray diffraction, scanning electron microscopy, electrochemical impedance spectroscopy and charge-discharge tests. The XRD results showed that the aluminum doped material with a mass fraction of 1% had a lower degree of cation mixing and a more stable structure. $Li(Ni_{0.6}Co_{0.2}Mn_{0.2})_{0.99}Al_{0.01}O_2$ cathode material provided a high discharge specific capacity of 181.82 $mAh\cdot g^{-1}$ at 0.1 C and maintained a capacity of about 92.60% after 100 cycles. When the current density was 2 C, it still retained a discharge specific capacity of 128.96 $mAh\cdot g^{-1}$, which was a huge improvement compared to that of pure $LiNi_{0.6}Co_{0.2}Mn_{0.2}O_2$. In general, it may be a good way to reduce the adverse environmental impact of landfilling spent lithium batteries by the sustainable recovery of high value-added metals in spent lithium ion batteries to synthesize new cathode materials.

Keywords: NCM622, Aluminum doping, Lithium ion batteries, Recycling

1. INTRODUCTION

Lithium ion batteries (LIBs) are widely used as power source in 3C field (computer, communication and consumer electronics) owing to their excellent electrochemical performance such as low self-discharge, high battery voltage and high energy density [1-4]. However, a majority of spent LIBs were discarded due to a sharp attenuation of discharge capacity after several years of service [5-7]. Because of the existence of heavy metals and organic compound in these spent LIBs, they can't be simply disposed of deep underground for sustainability and environmental reasons [1,8]. In addition, due to the limitation of natural resources and the growing demand for energy, it is necessary to recycle the valuable metals in spent LIBs [9-10].

In various LIBs cathode materials, layered nickel-rich $LiNi_xCo_yMn_{1-x-y}O_2$ (NCM, x ≥ 0.6) [11-13] is one of the most promising materials, which combines the advantages of $LiCoO_2$ [4,5,7,8], $LiNiO_2$ [14-15] and $LiMnO_2$ [16-18] by the synergy of the three elements. However, nickel-rich NCM materials have some defects such as poor cycling stability and rate capability under high voltage. In order to deal with these problems, researchers have confirmed that ion doping is an effective method such as doping titanium [19], zirconium [20], molybdenum [21], aluminum [22-23], magnesium [24] and other elements.

In this paper, the preparation and modification of $LiNi_{0.6}Co_{0.2}Mn_{0.2}O_2$ cathode materials with spent $LiCoO_2$ LIBs as lithium and cobalt source were studied. Moreover, the influence of aluminum doping on the microstructure and electrochemical performance of NCM622 cathode materials had also been researched.

2. EXPERIMENTAL

2.1 Cathode separation and leaching

The spent LIBs used in this paper were Xiaomi 3.85V polymer lithium ion mobile phone batteries collected from the local electronic market. To avoid the risk of short circuit, these LIBs were fully discharged in 1 $mol\cdot L^{-1}$ potassium chloride solution for 48 hours. Then the LIBs were manually dismantled into anode, cathode, separator and plastic shell in a fume hood. Following the cathode was immersed in 1 $mol\cdot L^{-1}$ sodium hydroxide solution for 2 hours in order to separate aluminum foil and cathode active material. After that, the residues were collected through filtration and then calcinated at 600 °C for 2 hours to remove polyvinylidene fluoride (PVDF) and acetylene black. Afterwards, acid leaching experiments with sulfuric acid and hydrogen peroxide were carried out. Later, the pH in the leachate was adjusted with sodium hydroxide to obtain cobalt hydroxide, and the lithium element in the filtrate was recovered in the form of lithium carbonate by saturated sodium carbonate solution.

2.2 Materials preparation

The recovered cobalt hydroxide was dissolved in sulfuric acid to obtain cobalt sulfate solution, and the pH of cobalt sulfate solution was adjusted to about 7 by sodium hydroxide. The $Ni_{0.6}Co_{0.2}Mn_{0.2}(OH)_2$ precursor was synthesized by co-precipitation process. First, 2 $mol\cdot L^{-1}$ mixed solution of cobalt sulfate, nickel sulfate and manganese sulfate (the molar ratio of Ni: Co: Mn = 6:2:2) was pumped into a continuous stirred tank, and 2 $mol\cdot L^{-1}$ sodium hydroxide and 1 $mol\cdot L^{-1}$ ammonia were simultaneously fed into the reactor. Then the reaction temperature was kept at 50 °C for 5 hours, and the pH of the solution was precisely controlled to 11 by the rate of sodium hydroxide addition. After filtration, the residue was washed several times, then dried at 80 °C for 12 hours. After that the obtained precursor was mixed with lithium carbonate to obtain pure NCM622, and aluminum doped NCM622 was synthesized from the mixture of the precursor, lithium carbonate and aluminum hydroxide. In addition, 5% excess of lithium carbonate was added to compensate for the loss of lithium during calcination process. Afterwards, the mixture was heated to 800 °C in a tube furnace at a heating rate of 5 °C·min^{-1} and maintained at 800 °C for 12 hours. Finally, $Li(Ni_{0.6}Co_{0.2}Mn_{0.2})_{1-x}Al_xO_2$ (x = 0, 0.005, 0.010, 0.015 and 0.020 named as NCM-0, NCM-0.5, NCM-1.0, NCM-1.5 and NCM-2.0) cathode materials would be obtained.

2.3 Characterization of the materials

The phase composition of samples was represented by X-ray powder diffraction (XRD, Shimadzu-9100) with Cu Ka radiation at 25 °C between 10° and 80°. In addition, the Jade software was used to calculate the crystal cell parameters for a general analysis. Moreover, the morphology of samples was characterized by a scanning electron microscopy (SEM, SU8000, Hitachi, Japan).

2.4 Electrochemical performance test for the materials

Electrochemical performance of the $LiNi_{0.6}Co_{0.2}Mn_{0.2}O_2$ was performed using half-type coin cells (LIR2016) with lithium foil as the negative electrode. First, the $LiNi_{0.6}Co_{0.2}Mn_{0.2}O_2$, PVDF and acetylene black (at a mass ratio of 8:1:1) were mixed and dispersed into NMP to obtain black uniform viscous slurry. Then the blended slurries were coated on an aluminum foil and dried at 100 °C in vacuum for 12 hours. After that circular electrodes were prepared by a punch cutting machine, and the mass load of $LiNi_{0.6}Co_{0.2}Mn_{0.2}O_2$ in the electrode was about 2 ± 0.3 mg·cm^{-2}. Afterwards, the battery was assembled in an argon atmosphere glove box, the polypropylene micro-porous film celgrad 2400 was used as separator and 1 mol·L^{-1} $LiPF_6$ dissolved in EC: EMC: DMC (1:1:1 in volume) was used as the electrolyte. Finally, electrochemical measurement was carried out at room temperature (25 °C) between 2.7 V and 4.3 V on a battery testing system (Shenzhen, NEWWARE instrument Co. Ltd., China).

3. RESULT AND DISSCUSSION

3.1 Acid leaching result

The XRD pattern of the cathode materials obtained from the spent lithium ion batteries after pretreatment is shown in Figure 1, which is completely consistent with the $LiCoO_2$ (JCPSD No.50–0653). Leaching procedure was carried out under the conditions of hydrogen peroxide concentration of 3 vol%, reaction time of 120 min, solid-liquid ratio of 40 g·L^{-1} and sulfuric acid concentration of 2 mol·L^{-1}. Then, lithium and cobalt ions are precipitated and separated as lithium carbonate and cobalt hydroxide after acid leaching, respectively. The leaching efficiency of Li and Co is 97.1% and 96.8%, respectively.

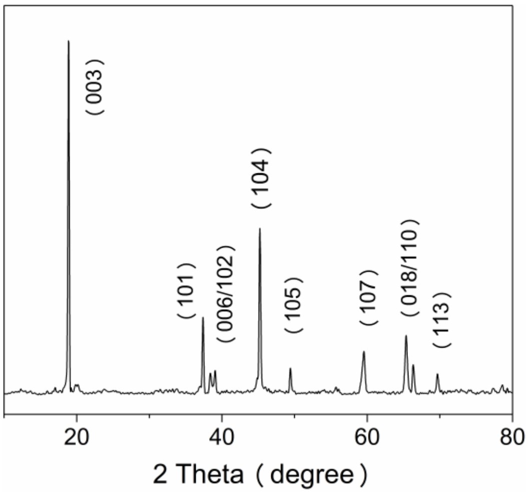

Figure 1. XRD patterns of $LiCoO_2$

3.2 Influence of aluminum doping on material structure

Obviously, the diffraction peaks of all the samples (as shown in Figure 2(a)) can be assigned to a layered hexagonal α-$NaFeO_2$ structure with space group R-3m without a visible impurity phase, which belongs to the layered $LiNiO_2$ (JCPSD No.09–0063). As can be seen from Figure 2(a), all materials have distinct and sharp characteristic peaks at 18.8, 36.6 and 44.4 degree, indicating that these materials have high crystallinity. In addition, Figure 2(b) shows the 003 peak of each material. It can be seen that the 003 peak of all aluminum-doped materials is shifted to a low angle, indicating that the cell spacing of the doped material increases [22]. Moreover, the detailed lattice parameters calculated from the XRD results are listed in Table 1. The intensity ratio of (003) and (104) peaks and c/a is often used to judge the mixing degree of Li^+ and Ni^{2+} cations in NCM materials, higher ratio means better ordering of NCM cations [21,25].

Table 1. The unit cell parameters c/a, I_{003}/I_{104} and R factor of NCM materials.

	NCM-0	NCM-0.5	NCM-1.0	NCM-1.5	NCM-2.0
I_{003}/I_{104}	1.25595	1.32637	1.40582	1.39534	1.35646
a	2.86678	2.86612	2.86501	2.86589	2.86512
c	14.20646	14.21042	14.20835	14.21150	14.20643
c/a	4.95555	4.95806	4.95926	4.95884	4.95840
R	0.46375	0.41342	0.43953	0.42187	0.41254

The ratio of I_{003}/I_{104} of NCM-0, NCM-0.5, NCM-1.0, NCM-1.5 and NCM-2.0 materials is 1.25595, 1.3267, 1.40582, 1.39534 and 1.35646, respectively, all of them are greater than 1.2, indicating that the cations of all samples are ordered. While the smaller value of R factor (referred to as $(I_{006}+I_{012})/I_{101}$) and the clear splitting of peaks (006)/(012) and (018)/(110) means the layered structure is more orderly[24]. The NCM-1.0 material has the largest value of c/a (4.95926) and I_{003}/I_{104} (1.40582) with a smaller R factor (0.43953), expressing that the NCM-1.0 material has a lowest degree of Li^+/Ni^{2+} mixing and an more order layered structure in the five samples. In general, compared with undoped materials, the proper amount of aluminum ion doping can effectively reduce the degree of cation mixing and make the layered structure more orderly.

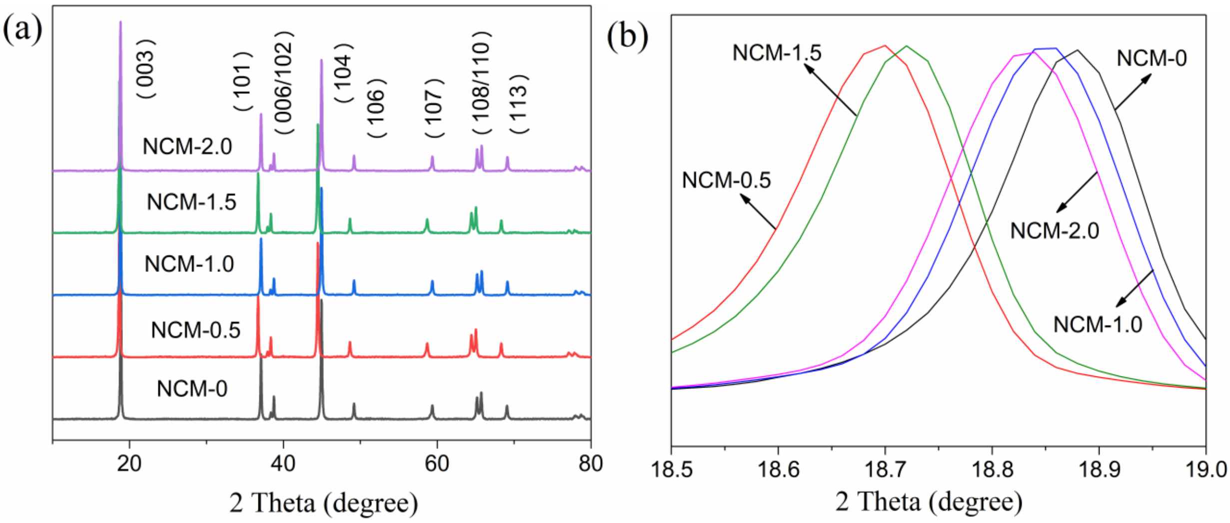

Figure 2. (a) XRD patterns of NCM materials and (b) enlarged XRD pattern at 18.5° – 19.0°

It can be obtained from the scanning graph (Figure 3(a)) that all materials exhibit spherical secondary particles, which are composed of small primary particles. Furthermore, it is obvious that all materials have a micron-sized porous spheres. The microsphere particles have many advantages, such as shortening the Li^+ diffusion path, reducing volume expansion/compression during charge and discharge, and contributing to electrolyte diffusion into the electrode material [26,27]. In addition, the primary structure difference between these materials can be seen from Figure 3(b-f). The interface of the doped material, especially NCM-1.0, is relatively clear and the secondary particles are obviously shown, while the interface of the undoped NCM-0 material is very vague.

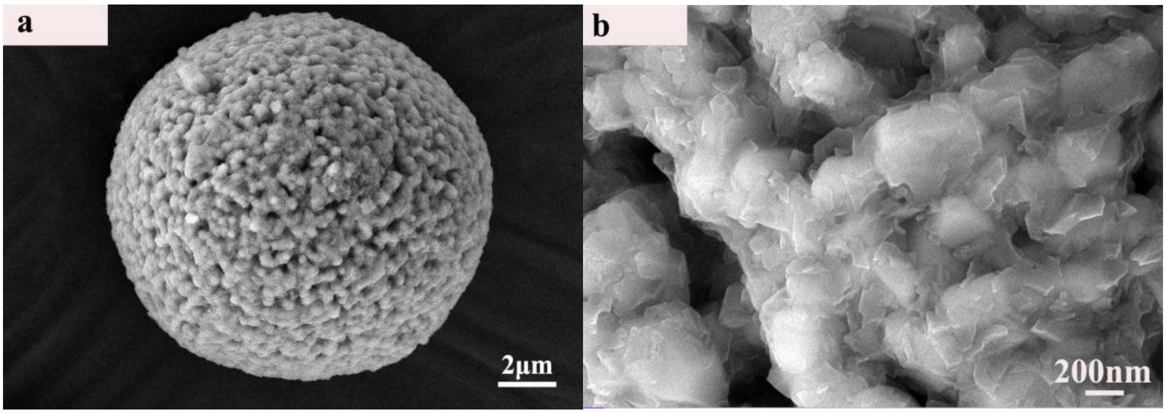

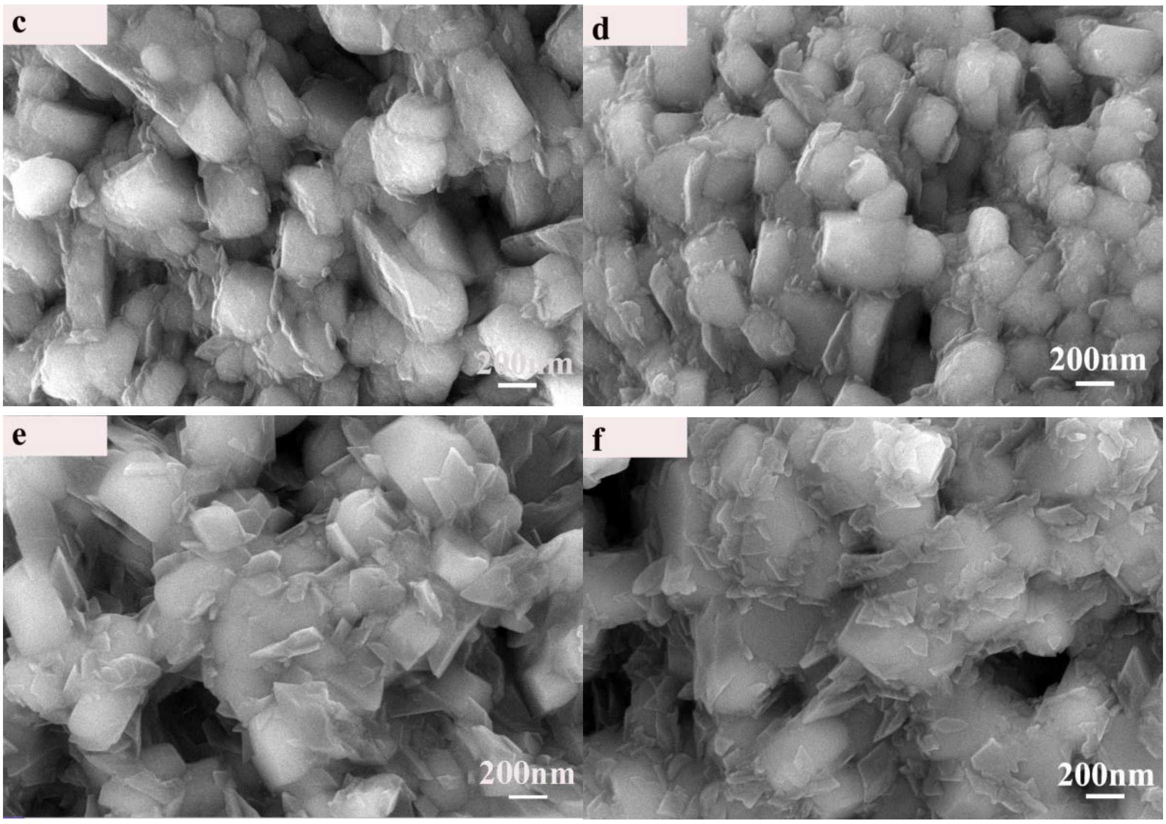

Figure 3. (a), (b) SEM images for NCM-0, (c) SEM images for NCM-0.5, (d) SEM images for NCM-1.0, (e) SEM images for NCM-1.5, (f) SEM images for NCM-2.0.

3.3 Influence of aluminum doping on electrochemical performance

Figure 4(a) shows cycling performance of the samples at 0.1 C. The initial discharge capacity of all samples is around 180 mAh·g^{-1}. After 100 cycles, the discharge capacity of LNCM-1.0 remains at 172.04 mAh·g^{-1}, while that of NCM-0, LNCM-0.5, LNCM-1.5 and LNCM-2.0 decays to 142.51, 151.87, 160.39 and 157.83 mAh·g^{-1}, respectively. In addition, the capacity retention of NCM-0, LNCM-0.5, LNCM-1.0, LNCM-1.5 and LNCM-2.0 is 79.17%, 84.37%, 95.58%, 89.10% and 87.68%, respectively. In Figure 4(b), the 100th cycle charge/discharge curves of NCM-0, NCM-0.5, NCM-1.0, NCM-1.5 and NCM-2.0 at 0.1 C are presented, respectively. Compared to the aluminum doping materials the discharge platform of the undoped materials discharge curve is significantly reduced. The results show that the incorporation of aluminum can effectively improve the cycle stability of $LiNi_{0.6}Co_{0.2}Mn_{0.2}O_2$ materials.

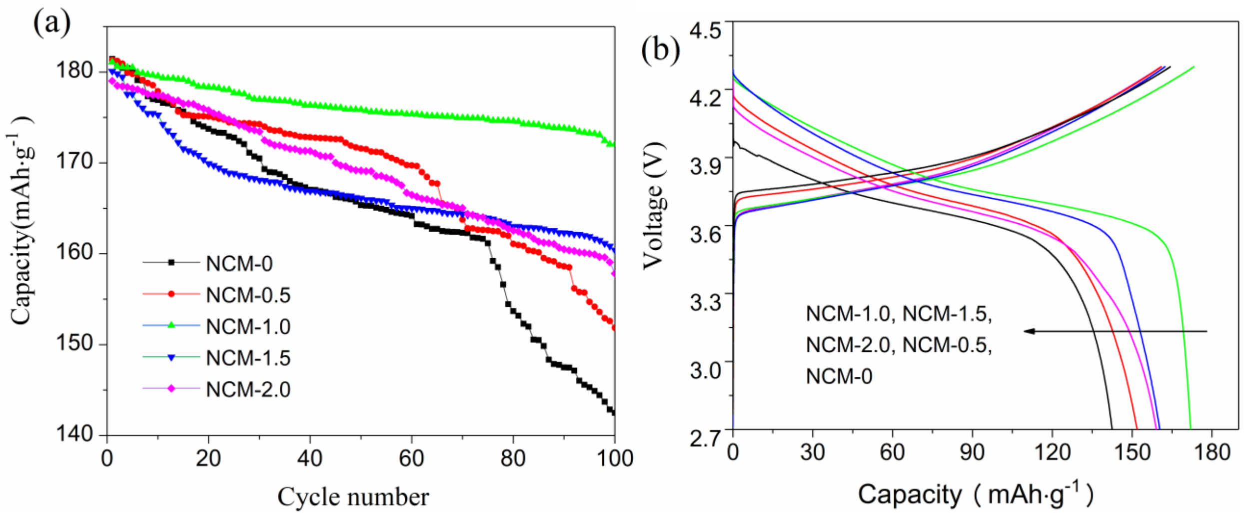

Figure 4. (a) the cycling performance of different doped materials at 0.1 C, (b) 100th charge-discharge curves of different doped materials.

The rate performance of all the prepared materials at 2.7-4.3 V voltage range is shown in Figure 5(a). At 2 C current density, the specific discharge capacity of NCM-1.0 is 128.96 mAh·g^{-1}, which is much higher than that of NCM-0 (75.06 mAh·g^{-1}). Therefore, it can be seen that aluminum doping improves the rate performance of the NCM622 materials. In addition, due to battery polarization, the capacity of all samples shows a significant attenuation with the increase of current density. It can be clearly presented from Figure 5(b), which demonstrates the charge and discharge curves of NCM-1.0 material at current densities of 0.1 C, 0.2 C, 0.5 C, 1 C and 2 C, respectively. It can be inferred that the excellent rate performance of aluminum-doped NCM622 material is due to the increase of lithium layer distance, which is beneficial to the transport of lithium ions [22].

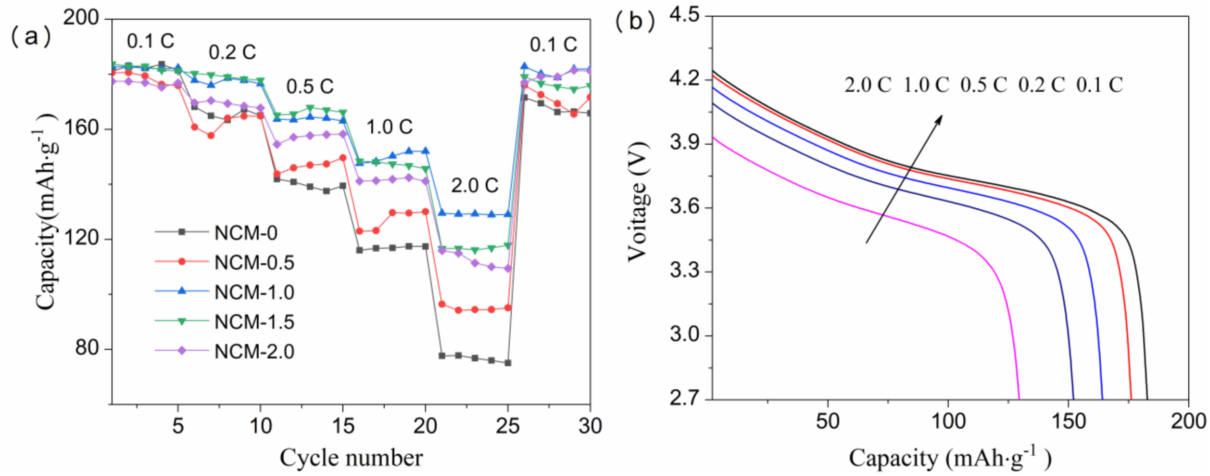

Figure 5. The rate performance of different doped materials: (a) rate capability at 0.1 C 0.2 C, 0.5 C, 1 C, 2 C in sequence for each 5 cycles, respectively, (b) discharge capacity at the first cycle under the variant rates for NCM-1 sample

In order to further study the influence of aluminum doping on the electrochemical properties of NCM622 materials, EIS (0.01 Hz–0.1 MHz, 5 mV perturbation) was performed on NCM-0, NCM-0.5, NCM-1.0, NCM-1.5 and NCM-2.0 electrode after 100 cycles in coin cell. The Nyquist plot is fitted and shown in Figure 6(a), where a semicircle associated with the charge transfer resistance of the electrode can be found, while the diagonal line of the low frequency region is related to the Li^+ diffusion within the electrode. In the equivalent electrical circuits Figure 6(b), R_s represents the solution ohmic resistance, R_e is the solid-electrolyte interface film resistance and R_{ct} corresponds to the charge transfer resistance [28,29]. In addition, CPE_1 refers to the constant phase element of the surface film, CPE_2 is assigned to the interfacial capacitance, and the Warburg impedance (Z_w) describing the diffusion of lithium ion in the bulk [22,30]. Furthermore, the Li^+ diffusion coefficient (D_{Li^+}) is considered as an important parameter for evaluating the electrochemical performance, and the equation used to calculate D_{Li^+} is as follows:

$$D = \frac{R \cdot T^2}{2 \cdot A^2 \cdot n^4 \cdot F^4 \cdot C^2 \cdot \delta^2}$$

In the formula, R is the ideal gas constant, T is the absolute temperature, A is the geometric area of electrode area, n is the number of electron transfer, F is the Faraday constant, C is the bulk phase concentration of lithium ions, and δ is the slope of the Z′(the real part impedance) and $\omega^{-1/2}$ (the angular frequency) curves in Figure 6(c) [28,30].

As shown in Table 2, in the five samples, the R_{ct} value of NCM-1.0 sample (283.58 Ω) is the lowest, while the Li^+ diffusion coefficient of NCM-1.0 (9.02 $X10^{-13}$) is significantly higher than that of other samples. It indicates that an appropriate amount (1%) of aluminum doping can improve the electrochemical kinetic behavior of the interface between the electrode and the electrolyte. In addition, we have made the electrochemical performance comparison between our as-prepared powder and other NCM materials for lithium-ion batteries previously reported. The results are summarized in Table 3, it is obvious that the NCM-1.0 material shows similar high reversible capacity compared with others.

Table 2. Fitting results for impedance spectra.

Sample	R_e(Ω)	R_s(Ω)	R_{ct}(Ω)	D_{Li^+}($cm^2\ s^{-1}$)
NCM-0	13.25	15.36	642.64	$1.12x10^{-13}$
NCM-0.5	13.13	15.97	404.03	$1.35x10^{-13}$
NCM-1.0	1.661	6.420	283.58	$9.02x10^{-13}$
NCM-1.5	5.671	9.2030	350.80	$6.50x10^{-13}$
NCM-2.0	7.504	10.17	369.83	$1.42x10^{-13}$

Table 3. Electrochemical performance comparison between NCM-1.0 and other NCM materials.

Sample	1st capacity (mAh·g^{-1})	Capacity retention (%)	Reference
NCM1	181.10	95.58 (100th cycle)	This work
Na-doped NCM	187.10	78.40 (30th cycle)	[11]

Ti-doped NCM	152.60	92.90 (50th cycle)	[19]
Zr-doped NCM	183.80	84.20 (60th cycle)	[20]
Mo-doped NCM	208.90	75.00 (100th cycle)	[21]

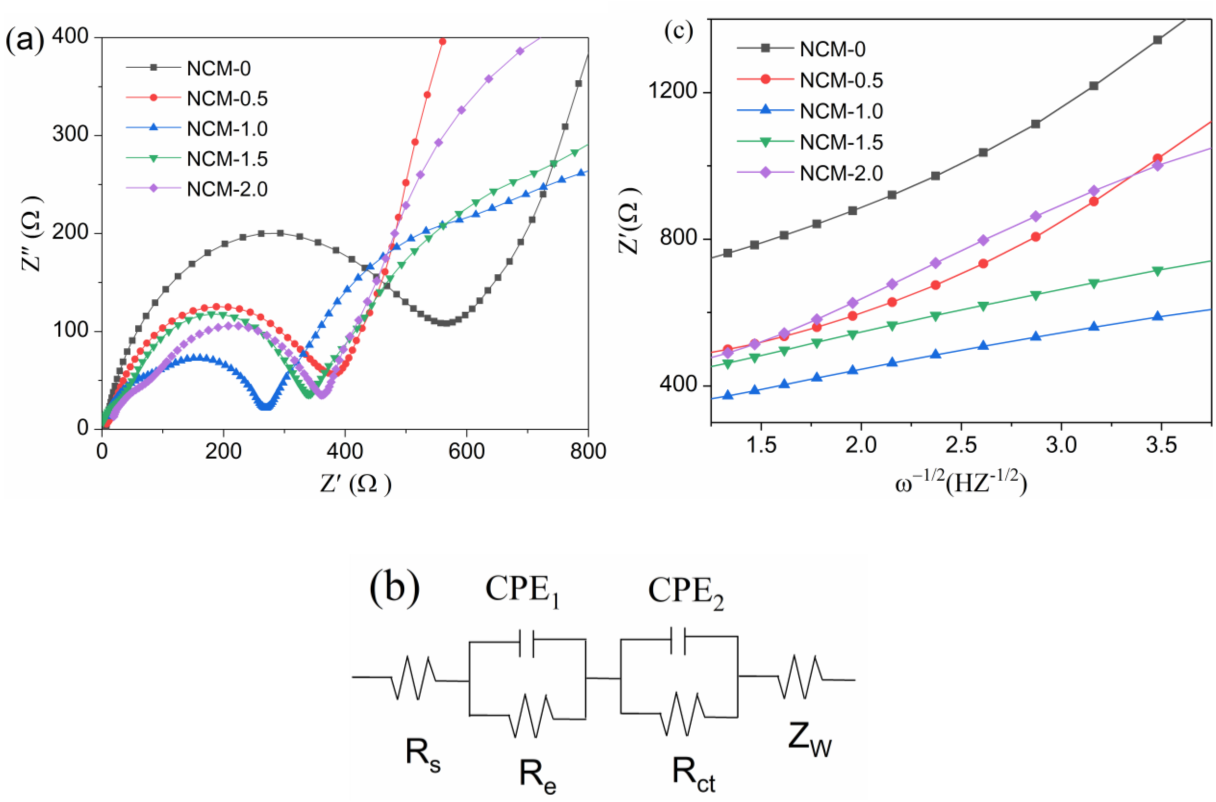

Figure 6. (a) Nyquist plots for the NCM electrodes at the 100th cycle, (b) equivalent circuit diagram, (c) the relation of $\omega^{-1/2}$ vs. Z′ after 100 cycles

4.CONCLUSION

This paper combines the recycling of spent $LiCoO_2$ batteries with the preparation of $LiNi_{0.6}Co_{0.2}Mn_{0.2}O_2$ cathode materials. On one hand, it reduces the environmental pollution caused by spent $LiCoO_2$ batteries. On the other hand, it makes full use of the lithium and cobalt resources to obtain high value-added products. The battery testing results show that when the content of the aluminum ion is 1%, the $Li(Ni_{0.6}Co_{0.2}Mn_{0.2})_{0.99}Al_{0.01}O_2$ material exhibits the best electrochemical performance.

References

1. E. G. Pinna, M. C. Ruiz, M. W. Ojeda, *Hydrometallurgy*, 167 (2017) 66.
2. J. Zhao, X. Qu, J. Qu, *J. Hazard. Mater.*, 379 (2019) 120817.
3. R. Jung, M. Metzger, F. Maglia, *J. Electrochem. Soc.*, 164 (2017) A1361.
4. V. C. B. Pegoretti, P. V. M. Dixini, P. C. Smecellato, *Mater. Res. Bull.*, 86 (2017) 5.
5. H. Chen, X. Zhu, Y. Chang, *Mater. Lett.*, 218 (2018) 40.
6. H. Ku, Y. Jung, M. Jo, *J. Hazard. Mater.*, 313 (2016) 138.
7. G. P. Nayaka, Y. Zhang, P. Dong, *Waste Manage. (Oxford)*, 78 (2018) 51.
8. L. E. Sita, S. P. da Silva, P. R. C. da Silva, *Mater. Chem. Phys.*, 194 (2017) 97.

9. X. Guo, X. Cao, G. Huang, *J. Environ. Manage.*, 198 (2017) 84.
10. Y. Tang, H. Xie, B. Zhang, *Waste Manage. (Oxford)*, 97 (2019) 140.
11. Y. Li, J. Liu, Y. Lei, *J. Mater. Sci.*, 52 (2017) 13596
12. X. Yao, Z. Xu, Z. Yao, *Mater. Today Commun.*, 19 (2019) 262.
13. Y. Ding, B. Deng, H. Wang, *J. Alloys Compd.*, 774 (2019) 451.
14. Y. Li, S. Deng, Y. Chen, *Electrochim. Acta*, 300 (2019) 26.
15. S. A. Song, H. T. Kim, K. Kim, *Int. J. Hydrogen Energy*, 44 (2019) 12085.
16. Q. Meng, J. Duan, Y. Zhang, *J. Ind. Eng. Chem.*, 80 (2019) 633.
17. Y. Yu, M. Xiang, J. Guo, *J. Colloid Interface Sci.*, 555 (2019) 64.
18. S. Bhuvaneswari, U. V. Varadaraju, R. Gopalan, *Electrochim. Acta*, 301 (2019) 342.
19. W. Cho, J. H. Song, K. W. Lee, *J. Phys. Chem. Solids*, 123 (2018) 271.
20. S. Gao, X. Zhan, Y. T. Cheng, *J. Power Sources*, 410 (2019) 45.
21. Q. Liu, Z. Zhao, F. Wu, *Solid State Ionics*, 337 (2019) 107.
22. L. Li, Z. Zhang, S. Fu, *J. Alloys Compd.*, 768 (2018) 582.
23. S. J. Do, P. Santhoshkumar, S. H. Kang, *Ceram. Int.*, 45 (2019) 6972.
24. X. Liu, S. Wang, L. Wang, *J. Power Sources*, 438 (2019) 227017.
25. B. Guo, J. Zhao, X. Fan, *Electrochim. Acta*, 236 (2017) 171.
26. F. Strauss, T. Bartsch, L. de Biasi, *ACS Energy Lett.*, 3 (2018) 992.
27. P. C. Tsai, B. Wen, M. Wolfman, *Energy Environ. Sci.*, 11 (2018) 860.
28. D. Zhang, Y. Liu, L. Wu, *Electrochim. Acta*, 328 (2019) 135086.
29. T. Tao, C. Chen, Y. Yao, *Ceram. Int.*, 43 (2017) 15173.
30. G. Sun, X. Yin, W. Yang, *Electrochim. Acta*, 272 (2018) 11.